

Moiré flat bands in twisted 2D hexagonal vdW materials

Qiaoling Xu,^{1,2} Yuzheng Guo,^{3,*} and Lede Xian^{2,4,†}

¹College of Physics and Electronic Engineering, Center for Computational Sciences, Sichuan Normal University, Chengdu 610068, China

²Songshan-Lake Materials Laboratory, Dongguan, Guangdong 523808, China

³School of Electrical Engineering and Automation, Wuhan University, Wuhan 430072, China

⁴Max Planck Institute for the Structure and Dynamics of Matter and Center
Free-Electron Laser Science, Luruper Chaussee 149, Hamburg 22761, Germany

(Dated: October 18, 2021)

Moiré superlattices in twisted bilayer graphene (TBG) and its derived structures can host exotic correlated quantum phenomena because the narrow moiré flat minibands in those systems effectively enhance the electron-electron interaction. Correlated phenomena are also observed in 2H-transitional metal dichalcogenides moiré superlattices. However, the number of moiré systems that have been explored in experiments are still very limited. Here we theoretically investigate a series of two-dimensional (2D) twisted bilayer hexagonal materials (TBHMs) beyond TBG at fixed angles of 7.34° and 67.34° with 22 2D van der Waals (vdW) layered materials that are commonly studied in experiments. First-principles calculations are employed to systemically study the moiré minibands in these systems. We find that flat bands with narrow bandwidth generally exist in these systems. Some of the systems such as twisted bilayer In_2Se_3 , InSe , GaSe , GaS and PtS_2 even host ultra-flat bands with bandwidth less than 20 meV even for such large angles, which make them especially appealing for further experimental investigations. We further analysis the characters of moiré flat bands and provides guidance for further exploration of 2D moiré superlattices that could host strong electron correlations.

I. INTRODUCTION

Moiré superlattice (MSL) is a special type of 2D layered material, generated by stacking 2D vdW materials with a small lattice mismatch or with a twist angle, including graphene, hexagonal boron nitride (hBN), transition metal dichalcogenides (TMDs), various 2D magnets and superconductors [1]. Different from their parent 2D materials, MSLs with emerging global symmetry and periodicity exhibit fascinating quantum phenomena due to periodic moiré modulation of onsite potentials, interlayer coupling and intralayer atomic strain, such as the formation of second-generation Dirac cones [2], Hofstadter butterfly states [3] and shear solitons and topological point defects [4–6].

Recent breakthroughs on the discovery of correlated insulator states and superconductivity in TBG [7, 8] have inspired intensive research on understanding the electronic structures [9–17], the correlated insulating phase, [9, 18, 19] and the mechanism of superconductivity [9, 18–23]. Moreover, novel quantum phenomena are found in TBG, such as correlation induced orbital magnetism [1, 24, 25] and quantum anomalous Hall states [26–29], cascades of phase transitions[30], Chern insulators [31, 32], and unconventional ferroelectricity [33, 34] etc. The exotic correlated properties of TBG are believed to be related to the emergence of the flat bands and the quenching of kinetic energy scales in those states when the twist angle is around the magic angles [35].

Following the success of TBG, a number of new moiré flat-band systems beyond TBG are explored, from the homobilayers, heterobilayers to multilayers configurations, including trilayer Graphene/hBN [36, 37], twisted double bilayer

graphene [38–44], twisted trilayer graphene [45–47], twisted monolayer–bilayer graphene [48–51] and twisted transition metal dichalcogenides (TMDs) [52–58] and so on. For example, Dai et al. [59] theoretically studied stacking configurations by the generic form of $(M + N)$ -layers TBG, where the N -layers graphene are stacked on top of M -layers graphene at a small twist angle and explore their electronic structures and topological properties. Here twisted double bilayer graphene, as one of the simplest example with $M = 2$, $N = 2$, has already been reported in experiments [38–40]. In view of TMDs, numerous stacking configurations with various combination (i.e, twisted $\text{MoS}_2/\text{MoS}_2$ [60, 61], $\text{WSe}_2/\text{WSe}_2$ [62, 63], WS_2/WS_2 [64], WS_2/WSe_2 [65], $\text{MoSe}_2/\text{WSe}_2$ [66–70], $\text{WS}_2/\text{MoSe}_2$ [71] etc.) are investigated. For instance, the 3D reconstructed WSe_2/WS_2 moiré superlattices with strain are found with the moiré flat bands by Crommie et al. recently [72]. Furthermore, Wang et al. reported a twisted bilayer WSe_2 at a small twist angle, where low-energy flat bands are observed and the correlated electronic phases are investigated [62].

Except for the typical materials of graphene-based and TMDs, the twisted bilayer black phosphorus [73] and grey antimonene [74] are also studied in structural and electronic properties respectively by Guo et al. More recently, Liu et al. investigated antiferro- and ferroelectric bilayer In_2Se_3 with large twist-angles [75] based on the first-principles calculations, where low-energy extremely flat band is found. Moreover, the studies of MSLs are further extended to the complex magnetic materials [76–79]. Balents et al. theoretically investigated the twisted bilayers of vdW magnets in the structures and phases [77], while Tong et al. considered the twisted bilayer 2D magnets CrX_3 ($X=\text{Br}, \text{I}$) from the magnetization textures aspect [76]. Furthermore, other moiré dimensionalities are also explored from quasi-one dimension [80] up to three dimension [81–83], which greatly extends the use of twistrionic in multi-dimensional systems.

* yguo@whu.edu.cn

† lede.xian@mpsdl.mpg.de

The highly tunable correlation and superconductivity properties of MSLs also make them appealing for future technology applications. A couple of the early attempts were made by Jarillo-Herrero et al. and Rickhaus et al., who made use of the gate-tunable correlated and superconductivity phase of magic angle TBG to fabricate Josephson junctions in single-crystal nanostructures [84, 85]. Moreover, Jarillo-Herrero et al. showed signatures of unconventional ferroelectricity in the bilayer graphene/boron nitride moiré system, which may lead to ultrafast, programmable and atomically thin carbon-based memory device applications [86].

The studies of the MSLs have provided powerful venue to explore the correlated physics and unconventional superconductivity [1, 87–89] as well as their applications in future technology. In the meanwhile, the emergence of thousands of new vdW layered materials [90] gives access to tremendous opportunities for the research of different types of MSLs. However, it remains unclear that whether moiré flat bands are generally exist in MSLs when the twist angle is small enough or the moiré periodic is large enough. Moreover, it is unclear what types of 2D materials are more susceptible to the formation of moiré flat bands and how one could find moiré flat band systems with a relatively large twist angle or small system size, which may potentially give rise to stronger electron-electron correlation and/or higher transition temperature for unconventional superconductivity. To address these questions, we perform first-principle calculations to study systematically 22 twisted homo-bilayer superlattices constructed with 2D materials that are accessible in experiments. We constraint our calculations to systems with twist angles at 7.34° and 67.34° as we want to look for moiré flat-band systems with small system size. By analyzing the band structures, we find bands with significantly reduced bandwidths generally exist in these MSLs. Interestingly, we do find a few MSLs that can host ultra-flat bands with bandwidth less than 20 meV even for such a large twist angle and small system size. Together with the relatively strong Hubbard interaction, these systems are expected to host strong electron-electron correlations, which is extremely appealing for further experimental investigation. We further discuss the band characters of the parent 2D materials that lead to the formation of the ultra-flat bands and provide guidance for future exploration of numerical exotic strongly-correlated MSLs.

II. MODEL AND COMPUTATIONAL APPROACHES

The present calculations are done within density functional theory (DFT) using the Vienna ab initio software package (VASP) [91]. For these configurations of 2D twisted superlattice, the exchange correlation functionals of Perdew Burke and Ernzerhof (PBE) [92] are used, in conjunction with Tkatchenko-Scheffler (TS) [93, 94] vdW corrections, which has been shown to give results well consistent with the experimental observations in our previous work on TMD-based MSLs [62]. An energy cutoff of 400 eV for the plane wave basis sets and the Γ -centered k-meshes of $1 \times 1 \times 1$ are used for geometry optimization and electronic structure calculations (a

$18 \times 18 \times 1$ k-grid is used for 1×1 unit cell). A vacuum thickness larger than 15 \AA is used to avoid artificial interactions between periodic slab images. All atoms are fully relaxed with residual force per atom less than 0.01 eV/\AA . Considering the computational cost of superlattice calculations, while the internal atomic positions are fully optimized, the lattice constant for moiré supercells is fixed to a value such that it corresponds to the experimental lattice constant for a 1×1 unit cell (See Table I for supercell lattice parameter for each MSL). For all calculations, due to the relativistic effect in heavy elements existing in most systems of TBHMs, the spin-orbit coupling (SOC) effect is considered while results without SOC are also calculated for comparison to estimate the effect of the SOC on the moiré flat bands.

For a wide variety of 2D materials, we concentrate on 22 types that are relatively easy to be synthesized and manipulated in experiments to construct twisted bilayer moiré superlattices. The composition and crystal structures for the corresponding bulk materials are shown in Fig. (1). These 2D materials range from two-atom-thick rhombohedral (grey) layered arsenic (As) and antimony (Sb) with spacegroup P63/mmc, three-atom-thick layers with octahedral (PtX_2 , PdX_2 , HfX_2 , ZrX_2 , SnX_2) with spacegroup P-3m1 or trigonal prismatic coordination (MoX_2 , WX_2) with spacegroup P63/mmc, four-atom-thick layers (GaS, GaSe, InSe) with space group R-3mH to five-atom-thick layers (Bi_2Se_3 , Bi_2Te_3 , In_2Se_3 , Sb_2Se_3) with spacegroup R-3mH (The details of structural data are presented in Table I). Moiré superlattices are obtained by rotating two identical layers from these parent 2D materials at a small angle. We consider TBHM models that have a moiré wavelength $\lambda(\theta_m) = a/(2 \sin(\theta_m/2))$ [95, 96]. For every commensurate twist angle θ_m , the supercell basis vectors are given by $t_1 = ma_1 + (m+1)a_2$ and $t_2 = -(m+1)a_1 + (2m+1)a_2$, where $a_{1,2} = (\pm 1/2, \sqrt{3}/2)a_0$ are the lattice vectors for the primitive cell of the untwisted system, a_0 is experimental lattice constant, and $\cos(\theta_m) = (3m^2 + 3m + 1/2)/(3m^2 + 3m + 1)$ with m being an integer. We study TBHM with twist angles at 7.34° and 67.34° that correspond to two distinct configurations when $m=4$. The largest system we study here has a total number of 610 atoms. A series of optimized twisted configurations can be seen in Figs. 2a, 3(a, e), 4(a, e), 5(a, d) and Figs. S1-S22(a, b) in the Supporting Information (SI).

III. RESULTS AND DISCUSSION

A. Flat bands and electronic correlation in MSLs

We calculate the band structures of the 22 MSLs at the PBE+TS level with and without SOC. The results are summarized in Table I and the detailed band structures can be found in the SI. Except for the two twisted metallic systems (i.e., twisted bilayer PdTe_2 and PtTe_2), we find bands with narrow bandwidths commonly appear at the band edges in these MSL systems regardless of the variety of band structures in the original untwisted form. This suggests moiré engineering via creating MSL is quite effective in general in creating flat or narrow bands in 2D semiconductor systems. For the metal-

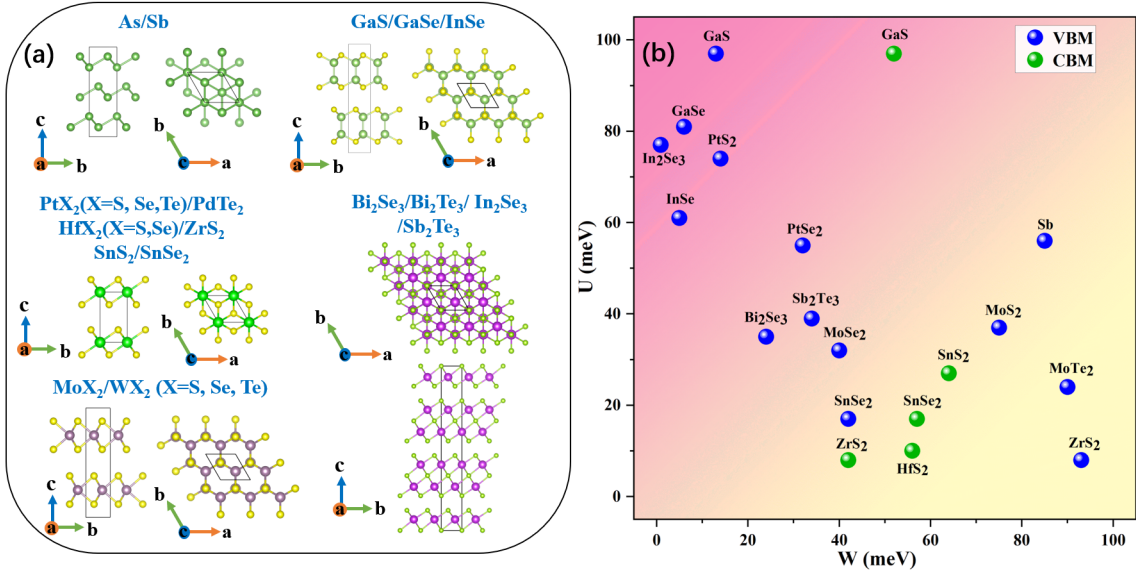


FIG. 1. (a) The composition and crystal structures of parent 3D vdW materials including two-atom-thick rhombohedral layered configuration (with the symmetry P6₃/mmc): As and Sb; three-atom-thick octahedral layered configuration (with the symmetry P-3m): PtX₂, PdX₂, HfX₂, ZrX₂ and SnX₂, or trigonal prismatic coordination (with the symmetry P6₃/mmc): MoX₂ and WX₂; four-atom-thick layers (with the symmetry R-3mH): GaS, GaSe and InSe; five-atom-thick layers (with the symmetry R-3mH): Bi₂Se₃, Bi₂Te₃, In₂Se₃ and Sb₂Te₃. (b) Distribution map of the TBHMs onto the variables of the on-site Hubbard interaction energy U vs bandwidth W with the scales of no more than 100 meV in VBM and CBM. The various twisted materials are marked. The color gradient from the top left (pink) to the bottom right (yellow) of the figure represents that effect of strong correlation varies from strong to weak.

TABLE I. The summary for the calculations of 2D twisted materials including: materials index (i), structural formula, moiré supercell lattice constant, average interlayer distance (D), bandwidths at the VBM (W-VBM) without (left) and with SOC (right), bandwidths at the CBM (W-CBM) without (left) and with SOC (right), relative permittivity (ϵ), on-site coulomb repulsion energy (U) and the projected orbitals at the VBM and CBM (only the top contributions listed), and the cohesive energy defined as the energy difference between the total energy of a bilayer with that of two well-separated monolayer in the primitive 1 \times 1 cell.

index(i)	struct.	lattice const. (\AA)	7.34°			67.34°			ϵ	U(meV)	orbital		cohesive energy (eV)
			Aver. D(A)	W-VBM(meV)	W-CBM(meV)	Aver. D(A)	W-VBM(meV)	W-CBM(meV)			VBM	CBM	
1	Bi ₂ Se ₃ [97]	32.295	3.185	21/24	n.a.	3.169	25/36	n.a.	12.8[98]	35	Se-p _z	Bi-p _z	0.23
2	In ₂ Se ₃ [99]	31.24	3.233	3/7	45/46	3.195	0.8/0.9	n.a.	6[100]	77	Se-p _z , Pt-p _z	In-s, p _z	0.25
3	Sb ₂ Te ₃ [101]	33.354	3.343	43/34	n.a.	3.340	45/57	n.a.	11[102]	39	Te-p _z	Sb-p _z	0.29
4	Bi ₂ Te ₃ [103]	34.283	3.376	n.a./18	n.a.	3.368	n.a./44	n.a.	n.a.	n.a.	Te-p _z	Bi-p _z	0.28
5	GaS[104]	28.054	3.320	n.a.	52/52	3.319	13/13	n.a.	5.397[105]	97	S-p _z /Ga-p _z	S-p _z /Ga-p _z , p _y	0.23
6	GaSe[106]	29.288	3.466	n.a.	n.a.	3.471	5/6	n.a.	6.1[105]	81	Se-p _z /Ga-p _z	Ga-s/Se-s, p _z	0.23
7	InSe[107]	31.269	3.305	n.a.	n.a.	3.311	n.a./5	n.a.	7.6[105]	61	Se-p _z /In-p _z	In-s/Se-s	0.24
8	As[108]	28.179	3.484	23/24	n.a.	3.490	n.a.	n.a.	n.a.	n.a.	As-p _z	As-p _z , s, p _z , p _y	0.15
9	Sb[109]	33.64	3.170	64/85	n.a.	3.188	n.a.	n.a.	8[110]	56	Sb-p _z /Sb-s, p _z , p _y	Sb-p _z , s, p _z , p _y	0.31
10	MoS ₂ [111]	24.681	3.140	n.a.	n.a.	3.160	75/75	n.a.	15.7[112]	37	Mo-d _{z²} /S-p _z	Mo-d _{z²} , d _{x²-y²}	0.31
11	MoSe ₂ [111]	25.687	3.311	n.a.	n.a.	3.340	40/40	n.a.	17.5[112]	32	Mo-d _{z²} /Se-p _z	Mo-d _{z²} , -y ² , d _{xy}	0.31
12	MoTe ₂ [113]	27.492	3.679	85/90	n.a.	3.688	73/100	n.a.	21.7[112]	24	Mo-d _{z²} -y ²	Mo-d _{z²} -y ² , d _{xy}	0.34
13	WS ₂ [114]	24.627	3.225	n.a.	n.a.	3.251	n.a.	n.a.	14.2[112]	41	W-d _{z²} /S-p _z	W-d _{z²} -y ² , d _{xy}	0.28
14	WSe ₂ [115]	25.664	3.391	160/191	n.a.	3.404	155/220	n.a.	15.7[112]	36	W-d _{z²} -y ² /Se-p _z , p _y	W-d _{z²} -y ² , d _{xy}	0.28
15	WTe ₂ [116]	27.265	3.750	130/161	n.a.	3.746	128/180	n.a.	n.a.	n.a.	W-d _{z²} -y ²	W-d _{z²} -y ² , d _{xy}	0.32
16	PdTe ₂ [117]	31.496	2.776	n.a.	n.a.	n.a.	n.a.	n.a.	n.a.	n.a.	n.a.	n.a.	0.53
17	PtS ₂ [118]	27.663	3.145	15/14	n.a.	3.179	n.a.	n.a.	7[119]	74	S-p _z /Pt-d _{z²} /S-p _z , p _y	Pt-d _{xy} , d _{z²} -y ² , d _{xy} , d _{yz}	0.24
18	PtSe ₂ [118]	29.108	3.138	32/32	n.a.	3.139	39/48	n.a.	9[119]	55	Se-p _z /Pt-d _{z²} /Se-p _z , p _y	Pt-d _{xy} , d _{z²} -y ² , d _{xy} , d _{yz}	0.28
19	PtTe ₂ [118]	31.436	2.96	n.a.	n.a.	n.a.	n.a.	n.a.	n.a.	n.a.	n.a.	n.a.	0.43
20	HfS ₂ [120]	28.359	3.097	n.a./158	55/56	3.109	n.a./160	60/60	51.3[112]	10	S-p _z , p _y /S-p _z	Hf-d _{z²} /S-p _z /Hf-d _{z²} , d _{z²} -y ² , d _{xy} , d _{yz}	0.30
21	HfSe ₂ [121]	29.243	3.227	n.a./276	76/76	3.224	n.a./274	79/80	n.a.	n.a.	Se-p _z , p _y	Hf-d _{z²} /Se-p _z /Hf-d _{z²} , d _{z²} -y ² , d _{xy} , d _{yz}	0.29
22	ZrS ₂ [122]	28.609	3.030	n.a./94	42/42	3.031	n.a./93	46/46	61.3[112]	8	S-p _z , p _y /S-p _z	Zr-d _{z²} /S-p _z /Zr-d _{z²} , d _{xy}	0.34
23	SnS ₂ [123]	28.413	3.349	n.a.	69/69	3.342	n.a.	64/64	18.8[124]	27	S-p _z , p _y	Sn-s/S-p _z , p _y	0.19
24	SnSe ₂ [125]	29.764	3.396	n.a./42	72/71	3.371	n.a.	57/57	28[126]	17	Se-p _z , p _y	Sn-s/Se-p _z , p _y , p _z	0.20

lic system, the bands near the Fermi level are highly entangled such that it is difficult to identify a well-defined flat band (see Fig. S23). We list the bandwidth of the flat bands appearing at the band edges in these systems in Table I. Not all systems have a value there either because for some systems the bands at the band edges are still quite dispersive (bandwidth $W > 200$ meV) or there is no well-defined isolated flat bands at the twist angles we study in this work. Furthermore, we calculate the unfolded band of PtSe_2 to further elaborate the moiré flat band. As shown in Fig. S25 of SI, the unfolded band structure (Fig. S25 (a)) in the twisted bilayer is drastically different from its counterpart (Fig. S25 (b)) in the untwisted structure. In particular, one can visualize a section of isolated flat band appearing at the VBM near the Γ point in the Brillouin zone of the primitive cell. This feature corresponds exactly to the flat bands that we calculated in the supercell Brillouin zone. The unfolded band structure reveals that the flat bands are originated from the linear recombination of the VBM states near the Γ point. Similar features of the flat bands have been observed in twisted bilayer graphene [127, 128] and WS_2/WSe_2 moiré superlattices [129]. From Table I, it is clear that it is easier to find flat bands at the VBM than at the CBM. For the flat bands at the VBM (CBM), the bandwidth ranges from 0.9 (42) meV to larger than 100 meV in our calculations with SOC. Nevertheless, it is surprising to find that the isolated band at the band edges in some twisted bilayer systems (such as twisted In_2Se_3 , GaSe , GaS , InSe , PtS_2) can be so flat that its bandwidth is less than 20 meV, even the twist angles we study here are relatively large.

The existence of flat bands in these MSLs indicates the kinetic energy scale of the electron states in these bands is significantly quenched and the electron-electron interaction and correlation may become important. To further evaluate the correlation effects, we estimate the on-site coulomb repulsion energy U in these system as $e^2/(4\pi\epsilon\epsilon_0 a)$, where e is electron charge, ϵ_0 is the vacuum permittivity, ϵ is relative permittivity and a is the effective linear dimension of each site (here we take the length scale of the moiré pattern). Though a combination of relative permittivity ϵ from the data of other literature and the lattice parameter of the moiré unite cell a , we estimate U and the values are depicted in Table I. Then, we compare the energy scale of the bandwidths W in VBM/CBM and estimated Hubbard U of different MSLs by plotting them in Fig. 1b (for MSLs with the same materials, only the smallest value of bandwidth is shown). In the region on the top left of Fig. 1b (colored in pink), the Hubbard U is larger than the bandwidth W , which indicates correlation effects will be important; while in bottom right region, the bandwidth W is larger and the electron correlation effect will be weak. Fig. 1b shows that the twisted compounds of GaS , GaSe , InSe , In_2Se_3 , PtS_2 all have narrow bandwidths and relative strong Hubbard interactions and they are expected to host strong electron correlations even at such a large twist angle of 7.34° . It is noteworthy that twisted arsenene should have a U value near that of antimonene, comparable or even more larger to its relatively small bandwidth of 24 meV, although we couldn't find the value of its ϵ in literature and didn't list it in the figure. The other systems near the diagonal line, such

as VBM of PtSe_2 , Bi_2Se_3 , Sb_2Te_3 and MoSe_2 and CBM of GaS , ZrS_2 , HfS_2 , SnS_2 and SnSe_2 , show comparable U and W values, indicating electron correlations are also important in these systems. For those systems locate at the lower right region in the diagram, such as MoTe_2 and ZrS_2 , the electron correlation may be less important. We need point out that we only compare the relevant energy scale for twisted systems at a relative large twist angle here, the locations of data points in this diagram (i.e., Fig. 1b) will change as the twist angle decreases. The twisted systems appear to have weaker electron correlations here could become strongly correlated systems at smaller angles.

B. Characters of the flat bands in MSLs

To better understand the formation of flat bands in 2D MSLs, we further analysis the characters of the flat bands. To this end, we conduct the calculation of the projected band structures and the results are shown in Figs. S1-S22 in the SI and the major orbital components for the states in the flat bands are summarized in Table I. The results reveal that for the flat band systems with smaller dispersion in VBM including the twisted materials of Bi_2Se_3 , In_2Se_3 , Sb_2Te_3 , Bi_2Te_3 , GaS , GaSe , InSe , PtS_2 and PtSe_2 , the valence band edges are associated with the p_z orbital of the chalcogen atom predominantly. Apart from these materials, the characters are also predominantly p_z orbitals for both of the twisted arsenene and antimonene in VBM. This is not surprising as we only study MSLs with a relatively large twist angle in this work, the atomic reconstruction has a minor effect. The moiré modulation of the band structure is dominated by the modulation of interlayer coupling, instead of the atomic reconstruction as reported in the work by Crommie and others [72] for MSLs with a much larger system size. Under such circumstance, as the electronic states with p_z orbital are very sensitive to the interlayer coupling, they can be significantly modified by the moiré potentials created by the modulated interlayer coupling and turned into flat-band states.

We take the twisted Bi_2Se_3 at 7.34° (Fig. 2a) as a typical example to further elaborate the role of different atomic orbitals in the formation of flat bands. The calculated band structure and the corresponding projected band structure of twisted Bi_2Se_3 are given in Fig. 2b and 2c. From these figures, it is clear that the states at the valence band edges are associated with Se p_z and a fraction of Bi s states. Whereas, the states at the conduction band edges are predominantly Bi p_z states. As the Se p_z orbitals are located at the outermost Se atomic layer, with charge density extended towards the stacking interface (See lower panels Fig. 2d), they are sensitive to the modulation of the interlayer coupling. Thus those states at the VBM, with relatively large contribution from Se p_z orbitals, are significantly altered by moiré interlayer potentials, forming a flat band with a small bandwidth of 21 meV. The charge density distribution of the states in this flat bands is very localized in the real space as shown in Fig. 2d. On the other hand, the Bi p_z orbitals locate at the inner atomic layers and their wavefunction barely extend towards to interface

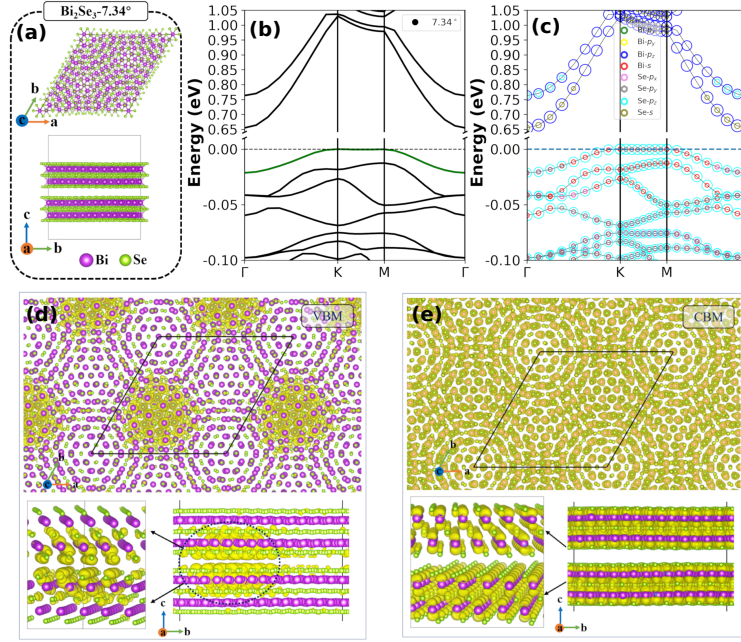


FIG. 2. Moiré flat bands in twisted bilayer Bi_2Se_3 at 7.34° . (a) Top view (upper panel) and side view (lower panel) of the atomic structure. The purple and green atoms represent Bi and Se atoms, respectively. (b) Low energy band structure near the band edges. (c) Low energy band structure with projection onto each atomic orbital. The size of the circle is proportional to the projection value. (d-e) Partial charge density distribution in real space for states at VBM (d) and CBM (e). Upper and lower panel show the top and the side views, respectively. The moiré unit cell is indicated by black solid lines. The dashed-line circle in the lower panel of (d) highlights the charge density localization region in Bi_2Se_3 . The isosurface value is set to be $7 \times 10^{-5} \text{ e}\text{\AA}^{-3}$.

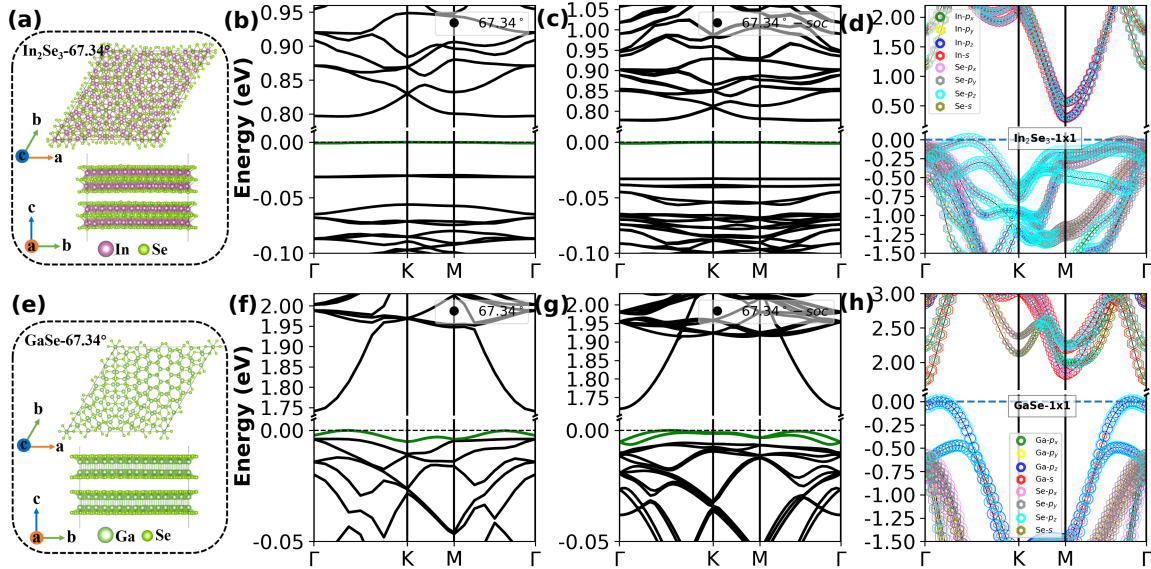


FIG. 3. (a) Top view (upper panel) and side view (lower panel) of the atomic structure of twisted bilayer In_2Se_3 at 67.34° . (b-c) Band structures for twisted bilayer without (b) and with (c) SOC. (d) Projected band structure for untwisted bilayer in 1×1 primitive cell without SOC. (e-h) The corresponding results for the GaSe systems.

region (see lower panel of Fig. 2e). Therefore, those states at the conduction band edge mainly contributed by the Bi p_z orbitals are much less sensitive to the modulation of interlayer couplings and the bands at the CBM are still very dispersive. The corresponding charge density distribution of those states is delocalized over the whole moiré cell as shown in Fig. 2e.

Next, we look at those systems that host flat bands with extremely small bandwidths even at a relatively large twist angle. Here, we investigate twisted bilayer In_2Se_3 and GaSe at 67.34° as two typical examples. As shown in Figs. 3b and 3f, the flat bands appear at the VBM with a extremely narrow bandwidth W of 0.8 and 5 meV for twisted bilayer In_2Se_3 and GaSe at 67.34° , respectively, in the calculations without SOC. When including SOC, the band structures of both systems have significant modifications: for the In_2Se_3 system, the band gap between the top and the lower flat bands increases and additional flat bands appear at higher energies; for the GaSe system, a Rashba type of splitting is introduced in the top flat band. Nevertheless, the bandwidths in both systems remain small after including SOC (0.9 meV for the In_2Se_3 system and 6 meV for the GaSe system). Similar to what we discussed above for the case of twisted Bi_2Se_3 , these ultra-flat bands states are mainly derived from the p_z orbital of the atoms in the outermost atomic layer (i.e., Se atoms in these cases), as shown in Fig. S24. Moreover, although the chemical composition and atomic structures are different, both systems share similar features in the band structure of the untwisted 1x1 form: that is, a relatively flat plateau at the VBM. This is also the case for the other ultra-flat band systems such as GaS and InSe. Such band plateau, when folded in the moiré supercell, naturally appears as flat bands. The moiré potential due to the modulated interlayer coupling further introduces band gaps between these flat bands at the supercell Brillouin Zone (BZ) boundary and confines those electronic states, leading to isolated ultra-flat bands. This is actually similar to the trilayer graphene/hBN moiré superlattice system [36, 37], where the states at the band plateau at the VBM are confined by the moiré potential formed by the graphene/hBN superlattice. As the band plateau region is more extended in the BZ in these systems, a much smaller moiré length scale is sufficient for the formation of ultra-flat bands. It is expected that the moiré heterostructures of these 2D layers could also host flat bands at the VBM.

Twisted bilayer PtS_2 is also an interest system. Different from the systems discussed above, although untwisted pristine bilayer PtS_2 does not has a flat band plateau at the band edges, its twisted form at 7.34° also host a ultra-flat band with a bandwidth of 15 meV in the calculation without SOC as shown Fig. 4b. The band structure doesn't change much when including SOC (see Fig. S16 in SI). Although the bandwidth is larger than the cases discussed above, it is still considerable small and comparable to the bandwidth of twist bilayer graphene at the magic angle of 1.05° , even at such a large twist angle. A noticeable feature in this twisted system is that the separation between flat bands is relatively large, indicating the strength of the interlayer moiré potential is relatively large. The relatively large moiré potential is likely to be related to the relatively strong interlayer hybridization of the S p_z states. As

shown in Fig. 4c and 4d, the S p_z states near the VBM in the untwisted bilayer have a considerable large energy splitting of about 1.5 eV compared with those in the monolayer, which even shifts the VBM from the S p_x - p_y states in the monolayer to the S p_z states in the untwisted bilayer. Another system that hosts relatively strong moiré potential is twisted bilayer buckled arsenene. As shown in Fig. 4g and 4h, the As p_z states near the VBM in the untwisted bilayer arsenene also have a relatively large energy splitting of about 1.0 eV, shifting the VBM from the As p_x - p_y states to the As p_z states. The twisted bilayer arsenene also hosts a large band gap between flat bands as shown in Fig. 4f.

Finally, we discuss the flat bands occurred at the CBM. Generally it is much harder to form flat bands at the CBM. Nevertheless, we found a few exceptions, such as twisted bilayer GaS, 1T-ZrS₂, HfS₂ and SnS₂. The band structures of twisted bilayer 1T-HfS₂ and GaS at 7.34° without including SOC effect are shown in Figs. 5b and 5e, respectively. The figures clearly show that isolated flat bands with similar shape appear at the bottom of the conduction bands in the two systems, with a bandwidth of 55 (52) meV for 1T-HfS₂ (GaS). The flat bands don't change much when the SOC effect is included (see Figs. S18 and S5 in the SI). A similar feature for these systems is that the bottom of the conduction bands of the pristine 1x1 bilayer locates at the M point in the BZ (see Fig. 5c and 5f). So the flat bands at the CBM of these systems are formed by the M point states. On the other hand, when the bottom of the conduction bands locate at the Gamma point, the bands at the CBM remain highly dispersive at large twist angles (see the previously discussed twisted bilayer Bi_2Se_3 and GaSe for example.).

IV. CONCLUSIONS

To summarize, we report a systematic investigation of band structures to explore flat bands in a series of 2D TBHMs with van der Waals beyond TBG using first-principles methods. Two configurations of moiré superlattice sharing supercells with the same size at twisted angles of 7.34° and 67.34° are considered. Our calculations show that the twisted compounds of Bi_2Se_3 , In_2Se_3 , Sb_2Te_3 , Bi_2Te_3 , GaS, GaSe, InSe, PtS_2 , PtSe_2 , arsenene and antimonene host flat bands at the VBM with the small bandwidths (less than 100 meV). Meanwhile, flat bands also emerge at the CBM for the twisted bilayer materials of GaS, HfS₂, HfSe₂, ZrS₂, SnS₂ and SnSe₂. Those systems that host flat bands at relatively large twist angles generally have the following characters: (1) The states at the band edges are mainly contributed by the outermost atoms of the layered materials and from those atomic orbitals where the charge density extends towards the stacking interface, such as p_z and d_{z^2} orbitals; (2) the band curvatures at around the band edges are relatively large or even relatively flat band plateaus appearing at the band edge in the Brillouin zone of the primitive cell. Then, by estimating the Hubbard interaction U , we find that the twisted compounds of Bi_2Se_3 , In_2Se_3 , GaS, GaSe, InSe and PtS_2 exhibit large Hubbard U over bandwidth W ratios, indicating electron correlation may

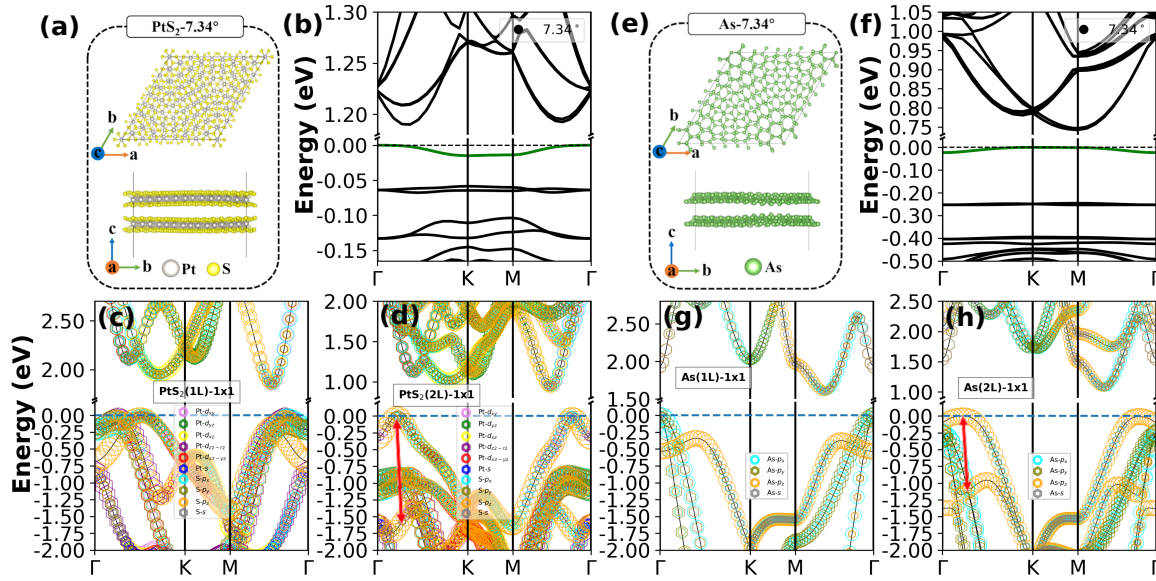


FIG. 4. (a) Top view (upper panel) and side view (lower panel) of the atomic structure of twisted bilayer PtS₂ at 7.34°. (b) Band structures for twisted bilayer without SOC. (c-d) Projected band structures for monolayer (c) and untwisted bilayer (d) in 1x1 primitive cell without SOC. The red arrows highlight the band splitting of the p_z states in the bilayer. (e-h) The corresponding results for the arsenene systems.

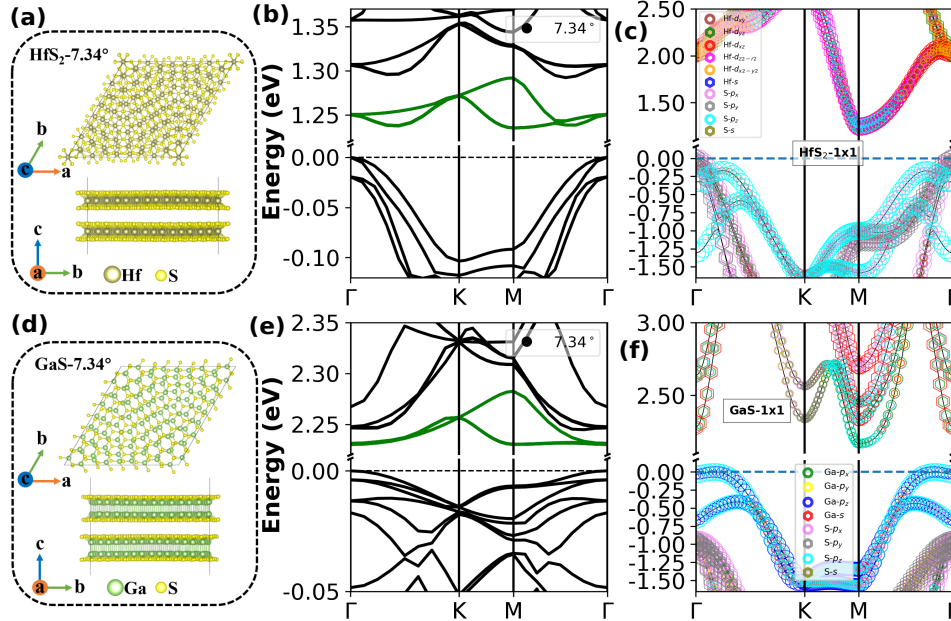


FIG. 5. (a) Top view (upper panel) and side view (lower panel) of the atomic structure of twisted bilayer HfS₂ at 7.34°. (b) Band structures for twisted bilayer without SOC. (c) Band structure for untwisted bilayer in 1x1 primitive cell without SOC. (d-f) The corresponding results for the GaS systems.

be relatively strong in those systems. Note that our study is limited to the systems with relatively large twist angles. When the twist angle further decreases and the system size becomes larger, flat bands may also appear in other systems, although for those systems the bands at the band edges are still quite dispersive at the angles we studied here. Nevertheless, the ultra-flat band systems we discuss here provide ideal candidates for the study of strong correlation effects at large twist angles. Finally, we discuss the characters of systems that host flat bands at large angles and provide a guideline for future exploration of novel 2D MSLs that host flat bands and potential

strong electron correlations.

V. ACKNOWLEDGEMENT

This work is supported by the Key-Area Research and Development Program of Guangdong Province of China (Grants No.2020B0101340001). The computational resource is provided by the Platform for Data-Driven Computational Materials Discovery of the Songshan Lake laboratory.

-
- [1] E. Y. Andrei, D. K. Efetov, P. Jarillo-Herrero, A. H. MacDonald, K. F. Mak, T. Senthil, E. Tutuc, A. Yazdani, and A. F. Young, *Nat Rev Mater* **6**, 201 (2021).
 - [2] E. Wang, X. Lu, S. Ding, W. Yao, M. Yan, G. Wan, K. Deng, S. Wang, G. Chen, L. Ma, J. Jung, A. V. Fedorov, Y. Zhang, G. Zhang, and S. Zhou, *Nature Phys* **12**, 1111 (2016).
 - [3] B. Hunt, J. D. Sanchez-Yamagishi, A. F. Young, M. Yankowitz, B. J. LeRoy, K. Watanabe, T. Taniguchi, P. Moon, M. Koshino, P. Jarillo-Herrero, and R. C. Ashoori, *Science* **340**, 1427 (2013).
 - [4] F. Gargiulo and O. V. Yazyev, *2D Mater.* **5**, 015019 (2017).
 - [5] M. M. v. Wijk, A. Schuring, M. I. Katsnelson, and A. Fasolino, *2D Mater.* **2**, 034010 (2015).
 - [6] J. S. Alden, A. W. Tsien, P. Y. Huang, R. Hovden, L. Brown, J. Park, D. A. Muller, and P. L. McEuen, *PNAS* **110**, 11256 (2013).
 - [7] Y. Cao, V. Fatemi, A. Demir, S. Fang, S. L. Tomarken, J. Y. Luo, J. D. Sanchez-Yamagishi, K. Watanabe, T. Taniguchi, E. Kaxiras, R. C. Ashoori, and P. Jarillo-Herrero, *Nature* **556**, 80 (2018).
 - [8] Y. Cao, V. Fatemi, S. Fang, K. Watanabe, T. Taniguchi, E. Kaxiras, and P. Jarillo-Herrero, *Nature* **556**, 43 (2018).
 - [9] H. C. Po, L. Zou, A. Vishwanath, and T. Senthil, *Physical Review X* **8**, 031089 (2018).
 - [10] N. F. Yuan and L. Fu, *Physical Review B* **98**, 045103 (2018).
 - [11] M. Koshino, N. F. Yuan, T. Koretsune, M. Ochi, K. Kuroki, and L. Fu, *Physical Review X* **8**, 031087 (2018).
 - [12] J. Kang and O. Vafek, *Physical Review X* **8**, 031088 (2018).
 - [13] Z. Song, Z. Wang, W. Shi, G. Li, C. Fang, and B. A. Bernevig, *Physical review letters* **123**, 036401 (2019).
 - [14] H. C. Po, L. Zou, T. Senthil, and A. Vishwanath, *Physical Review B* **99**, 195455 (2019).
 - [15] G. Tarnopolsky, A. J. Kruchkov, and A. Vishwanath, *Physical review letters* **122**, 106405 (2019).
 - [16] H. K. Pal, S. Spitz, and M. Kindermann, *Physical review letters* **123**, 186402 (2019).
 - [17] Y.-H. Zhang, D. Mao, and T. Senthil, *Physical Review Research* **1**, 033126 (2019).
 - [18] H. Isobe, N. F. Yuan, and L. Fu, *Physical Review X* **8**, 041041 (2018).
 - [19] C.-C. Liu, L.-D. Zhang, W.-Q. Chen, and F. Yang, *Physical review letters* **121**, 217001 (2018).
 - [20] C. Xu and L. Balents, *Physical review letters* **121**, 087001 (2018).
 - [21] F. Wu, A. MacDonald, and I. Martin, *Physical review letters* **121**, 257001 (2018).
 - [22] B. Lian, Z. Wang, and B. A. Bernevig, *Physical review letters* **122**, 257002 (2019).
 - [23] B. Roy and V. Jurić, *Physical Review B* **99**, 121407 (2019).
 - [24] J. Liu and X. Dai, *Nat Rev Phys* **3**, 367 (2021).
 - [25] X. Lu, P. Stepanov, W. Yang, M. Xie, M. A. Aamir, I. Das, C. Urgell, K. Watanabe, T. Taniguchi, G. Zhang, A. Bachtold, A. H. MacDonald, and D. K. Efetov, *Nature* **574**, 653 (2019).
 - [26] M. Serlin, C. L. Tschirhart, H. Polshyn, Y. Zhang, J. Zhu, K. Watanabe, T. Taniguchi, L. Balents, and A. F. Young, *Science* **367**, 900 (2020).
 - [27] F. Wu and S. Das Sarma, *Phys. Rev. Lett.* **124**, 046403 (2020).
 - [28] J. Liu and X. Dai, *Phys. Rev. B* **103**, 035427 (2021).
 - [29] J. Shi, J. Zhu, and A. H. MacDonald, *Phys. Rev. B* **103** (2021).
 - [30] U. Zondiner, A. Rozen, D. Rodan-Legrain, Y. Cao, R. Queiroz, T. Taniguchi, K. Watanabe, Y. Oreg, F. von Oppen, A. Stern, *et al.*, *Nature* **582**, 203 (2020).
 - [31] G. Chen, A. L. Sharpe, E. J. Fox, Y.-H. Zhang, S. Wang, L. Jiang, B. Lyu, H. Li, K. Watanabe, T. Taniguchi, Z. Shi, T. Senthil, D. Goldhaber-Gordon, Y. Zhang, and F. Wang, *Nature* **579**, 56 (2020).
 - [32] A. Abouelkomsan, Z. Liu, and E. J. Bergholtz, *Phys. Rev. Lett.* **124**, 106803 (2020).
 - [33] Z. Zheng, Q. Ma, Z. Bi, S. de la Barrera, M.-H. Liu, N. Mao, Y. Zhang, N. Kiper, K. Watanabe, T. Taniguchi, J. Kong, W. A. Tisdale, R. Ashoori, N. Gedik, L. Fu, S.-Y. Xu, and P. Jarillo-Herrero, *Nature* **588**, 71 (2020).
 - [34] K. Yasuda, X. Wang, K. Watanabe, T. Taniguchi, and P. Jarillo-Herrero, *Science* **372**, 1458 (2021).
 - [35] R. Bistritzer and A. H. MacDonald, *Proc. Natl. Acad. Sci. U.S.A.* **108**, 12233 (2011).
 - [36] G. Chen, A. L. Sharpe, P. Gallagher, I. T. Rosen, E. J. Fox, L. Jiang, B. Lyu, H. Li, K. Watanabe, T. Taniguchi, J. Jung, Z. Shi, D. Goldhaber-Gordon, Y. Zhang, and F. Wang, *Nature* **572**, 215 (2019).
 - [37] G. Chen, L. Jiang, S. Wu, B. Lyu, H. Li, B. L. Chittari, K. Watanabe, T. Taniguchi, Z. Shi, J. Jung, Y. Zhang, and F. Wang, *Nat. Phys.* **15**, 237 (2019).
 - [38] X. Liu, Z. Hao, E. Khalaf, J. Y. Lee, Y. Ronen, H. Yoo, D. H. Najafabadi, K. Watanabe, T. Taniguchi, A. Vishwanath, *et al.*, *Nature* **583**, 221 (2020), study of twisted double bilayer graphene which established correlated insulating and superconducting behavior.
 - [39] C. Shen, Y. Chu, Q. Wu, N. Li, S. Wang, Y. Zhao, J. Tang, J. Liu, J. Tian, K. Watanabe, *et al.*, *Nature Physics* **16**, 520 (2020).
 - [40] Y. Cao, D. Rodan-Legrain, O. Rubies-Bigorda, J. M. Park, K. Watanabe, T. Taniguchi, and P. Jarillo-Herrero, *Nature* **583**, 215 (2020).
 - [41] J. Y. Lee, E. Khalaf, S. Liu, X. Liu, Z. Hao, P. Kim, and A. Vishwanath, *Nature communications* **10**, 1 (2019).

- [42] G. W. Burg, J. Zhu, T. Taniguchi, K. Watanabe, A. H. MacDonald, and E. Tutuc, *Phys. Rev. Lett.* **123**, 197702 (2019).
- [43] M. He, Y. Li, J. Cai, Y. Liu, K. Watanabe, T. Taniguchi, X. Xu, and M. Yankowitz, *Nat. Phys.* (2020).
- [44] C. Zhang, T. Zhu, S. Kahn, S. Li, B. Yang, C. Herbig, X. Wu, H. Li, K. Watanabe, T. Taniguchi, S. Cabrini, A. Zettl, M. P. Zaletel, F. Wang, and M. F. Crommie, *Nat Commun* **12**, 2516 (2021).
- [45] J. M. Park, Y. Cao, K. Watanabe, T. Taniguchi, and P. Jarillo-Herrero, *Nature* **590**, 249 (2021).
- [46] Z. Zhu, S. Carr, D. Massatt, M. Luskin, and E. Kaxiras, *Physical review letters* **125**, 116404 (2020).
- [47] E. S. Morell, M. Pacheco, L. Chico, and L. Brey, *Physical Review B* **87**, 125414 (2013).
- [48] Y. Park, B. L. Chittari, and J. Jung, *Physical Review B* **102**, 035411 (2020).
- [49] S. Chen, M. He, Y.-H. Zhang, V. Hsieh, Z. Fei, K. Watanabe, T. Taniguchi, D. H. Cobden, X. Xu, C. R. Dean, *et al.*, *Nature Physics* **17**, 374 (2021).
- [50] L. Rademaker, I. V. Protopopov, and D. A. Abanin, *Physical Review Research* **2**, 033150 (2020).
- [51] S. Xu, M. M. Al Ezzi, N. Balakrishnan, A. Garcia-Ruiz, B. Tsim, C. Mullan, J. Barrier, N. Xin, B. A. Piot, T. Taniguchi, *et al.*, *Nature Physics* **17**, 619 (2021).
- [52] J. Kang, J. Li, S.-S. Li, J.-B. Xia, and L.-W. Wang, *Nano letters* **13**, 5485 (2013).
- [53] M. H. Naik and M. Jain, *Phys. Rev. Lett.* **121**, 266401 (2018).
- [54] F. Wu, T. Lovorn, E. Tutuc, and A. H. MacDonald, *Phys. Rev. Lett.* **121**, 026402 (2018).
- [55] F. Wu, T. Lovorn, E. Tutuc, I. Martin, and A. H. MacDonald, *Phys. Rev. Lett.* **122**, 086402 (2019).
- [56] Y. Zhang, N. F. Yuan, and L. Fu, *Physical Review B* **102**, 201115 (2020).
- [57] E. C. Regan, D. Wang, C. Jin, M. I. B. Utama, B. Gao, X. Wei, S. Zhao, W. Zhao, Z. Zhang, K. Yumigeta, M. Blei, J. D. Carlström, K. Watanabe, T. Taniguchi, S. Tongay, M. Crommie, A. Zettl, and F. Wang, *Nature* **579**, 359 (2020), study demonstrating Mott and generalized Wigner crystal states in WSe_2/WS_2 moiré superlattices.
- [58] Y. Tang, L. Li, T. Li, Y. Xu, S. Liu, K. Barmak, K. Watanabe, T. Taniguchi, A. H. MacDonald, J. Shan, and K. F. Mak, *Nature* **579**, 353 (2020), a work proposing the realization of Hubbard model physics in WSe_2/WS_2 moiré superlattices.
- [59] J. Liu, Z. Ma, J. Gao, and X. Dai, *Physical Review X* **9**, 031021 (2019).
- [60] L. Xian, M. Claassen, D. Kiese, M. M. Scherer, S. Trebst, D. M. Kennes, and A. Rubio, *Nature Communications* **12**, 1 (2021).
- [61] M. Angeli and A. H. MacDonald, *Proceedings of the National Academy of Sciences* **118** (2021).
- [62] L. Wang, E.-M. Shih, A. Ghiotto, L. Xian, D. A. Rhodes, C. Tan, M. Claassen, D. M. Kennes, Y. Bai, B. Kim, *et al.*, *Nature materials* **19**, 861 (2020).
- [63] Z. Zhang, Y. Wang, K. Watanabe, T. Taniguchi, K. Ueno, E. Tutuc, and B. J. LeRoy, *Nature Physics* **16**, 1093 (2020).
- [64] M. Liao, Z. Wei, L. Du, Q. Wang, J. Tang, H. Yu, F. Wu, J. Zhao, X. Xu, B. Han, *et al.*, *Nature communications* **11**, 1 (2020).
- [65] L. Yuan, B. Zheng, J. Kunstmann, T. Brumme, A. B. Kuc, C. Ma, S. Deng, D. Blach, A. Pan, and L. Huang, *Nature materials* **19**, 617 (2020).
- [66] K. L. Seyler, P. Rivera, H. Yu, N. P. Wilson, E. L. Ray, D. G. Mandrus, J. Yan, W. Yao, and X. Xu, *Nature* **567**, 66 (2019).
- [67] K. Tran, G. Moody, F. Wu, X. Lu, J. Choi, K. Kim, A. Rai, D. A. Sanchez, J. Quan, A. Singh, *et al.*, *Nature* **567**, 71 (2019).
- [68] M. Brotons-Gisbert, H. Baek, A. Molina-Sánchez, A. Campbell, E. Scerri, D. White, K. Watanabe, T. Taniguchi, C. Bonato, and B. D. Gerardot, *Nature Materials* **19**, 630 (2020).
- [69] M. R. Rosenberger, H.-J. Chuang, M. Phillips, V. P. Oleshko, K. M. McCreary, S. V. Sivaram, C. S. Hellberg, and B. T. Jonker, *ACS nano* **14**, 4550 (2020).
- [70] Y. Bai, L. Zhou, J. Wang, W. Wu, L. J. McGilly, D. Halberthal, C. F. B. Lo, F. Liu, J. Ardelean, P. Rivera, *et al.*, *Nature Materials* **19**, 1068 (2020).
- [71] L. Zhang, Z. Zhang, F. Wu, D. Wang, R. Gogna, S. Hou, K. Watanabe, T. Taniguchi, K. Kulkarni, T. Kuo, *et al.*, *Nature communications* **11**, 1 (2020).
- [72] H. Li, S. Li, M. H. Naik, J. Xie, X. Li, J. Wang, E. Regan, D. Wang, W. Zhao, S. Zhao, S. Kahn, K. Yumigeta, M. Blei, T. Taniguchi, K. Watanabe, S. Tongay, A. Zettl, S. G. Louie, F. Wang, and M. F. Crommie, *Nat. Mater.* **20**, 945 (2021).
- [73] P. Kang, W.-T. Zhang, V. Michaud-Rioux, X.-H. Kong, C. Hu, G.-H. Yu, and H. Guo, *Physical Review B* **96**, 195406 (2017).
- [74] Q. An, O. Moutanabbir, and H. Guo, *Nanoscale* (2021).
- [75] C. F. Li, W. J. Zhai, Y. Q. Li, Y. S. Tang, J. H. Zhang, P. Z. Chen, G. Z. Zhou, X. M. Cui, L. Lin, Z. B. Yan, X. K. Huang, X. P. Jiang, and J.-M. Liu, *New J. Phys.* **23**, 083019 (2021).
- [76] F. Xiao, K. Chen, and Q. Tong, *Physical Review Research* **3**, 013027 (2021).
- [77] K. Hejazi, Z.-X. Luo, and L. Balents, *Proceedings of the National Academy of Sciences* **117**, 10721 (2020).
- [78] C. Wang, Y. Gao, H. Lv, X. Xu, and D. Xiao, *Physical Review Letters* **125**, 247201 (2020).
- [79] Y.-H. Li and R. Cheng, *Physical Review B* **102**, 094404 (2020).
- [80] D. M. Kennes, L. Xian, M. Claassen, and A. Rubio, *Nature communications* **11**, 1 (2020).
- [81] F. Wu, R.-X. Zhang, and S. D. Sarma, *Physical Review Research* **2**, 022010 (2020).
- [82] L. Xian, A. Fischer, M. Claassen, J. Zhang, A. Rubio, and D. M. Kennes, *Nano letters* **21**, 7519 (2021).
- [83] Z. Song, X. Sun, and L.-W. Wang, *Physical Review B* **103**, 245206 (2021).
- [84] D. Rodan-Legrain, Y. Cao, J. M. Park, C. Sergio, M. T. Rande-ria, K. Watanabe, T. Taniguchi, and P. Jarillo-Herrero, *Nature Nanotechnology* **16**, 769 (2021).
- [85] F. K. de Vries, E. Portolés, G. Zheng, T. Taniguchi, K. Watanabe, T. Ihn, K. Ensslin, and P. Rickhaus, *Nature Nanotechnology* **16**, 760 (2021).
- [86] Z. Zheng, Q. Ma, Z. Bi, S. de la Barrera, M.-H. Liu, N. Mao, Y. Zhang, N. Kiper, K. Watanabe, T. Taniguchi, *et al.*, *Nature* **588**, 71 (2020).
- [87] D. M. Kennes, M. Claassen, L. Xian, A. Georges, A. J. Millis, J. Hone, C. R. Dean, D. N. Basov, A. N. Pasupathy, and A. Rubio, *Nat. Phys.* **17**, 155 (2021).
- [88] F. He, Y. Zhou, Z. Ye, S.-H. Cho, J. Jeong, X. Meng, and Y. Wang, *ACS Nano* **15**, 5944 (2021).
- [89] L. J. McGilly, A. Kerelsky, N. R. Finney, K. Shapovalov, E.-M. Shih, A. Ghiotto, Y. Zeng, S. L. Moore, W. Wu, Y. Bai, *et al.*, *Nature Nanotechnology* **15**, 580 (2020).
- [90] N. Mounet, M. Gibertini, P. Schwaller, D. Campi, A. Merkys, A. Marrazzo, T. Sohler, I. E. Castelli, A. Cepellotti, G. Pizzi, *et al.*, *Nature nanotechnology* **13**, 246 (2018).
- [91] G. Kresse and J. Furthmüller, *Phys. Rev. B* **54**, 11169 (1996).
- [92] P. E. Blöchl, *Phys. Rev. B* **50**, 17953 (1994).

- [93] A. Tkatchenko and M. Scheffler, *Phys. Rev. Lett.* **102**, 073005 (2009).
- [94] O. Anatole von Lilienfeld and A. Tkatchenko, *J. Chem. Phys.* **132**, 234109 (2010).
- [95] J. M. B. Lopes dos Santos, N. M. R. Peres, and A. H. Castro Neto, *Phys. Rev. Lett.* **99**, 256802 (2007).
- [96] E. J. Mele, *Phys. Rev. B* **81**, 161405 (2010).
- [97] C. Pérez Vicente, J. L. Tirado, K. Adoubay, J. C. Jumas, A. A. Touré, and G. Kra, *Inorg. Chem.* **38**, 2131 (1999).
- [98] M. Fang, Z. Wang, H. Gu, M. Tong, B. Song, X. Xie, T. Zhou, X. Chen, H. Jiang, T. Jiang, and S. Liu, *Applied Surface Science* **509**, 144822 (2020).
- [99] M. Kupers, P. M. Konze, A. Meledin, J. Mayer, U. Englert, M. Wuttig, and R. Dronskowski, *Inorganic chemistry* **57**, 11775 (2018).
- [100] D. Wu, A. J. Pak, Y. Liu, Y. Zhou, X. Wu, Y. Zhu, M. Lin, Y. Han, Y. Ren, H. Peng, Y.-H. Tsai, G. S. Hwang, and K. Lai, *Nano Lett.* **15**, 8136 (2015).
- [101] K. A. Kokh, V. Atuchin, T. Gavrilova, N. Kuratieva, N. Perukhina, and N. Surovtsev, *Solid state communications* **177**, 16 (2014).
- [102] B. Xu, Y. Cao, X. An, J. Zhang, S. Ma, Y. Wang, J. Chen, L. Chen, and L. Yi, *J. Phys. Soc. Jpn.* **88**, 124712 (2019).
- [103] V. Atuchin, T. Gavrilova, K. Kokh, N. Kuratieva, N. Perukhina, and N. Surovtsev, *Solid state communications* **152**, 1119 (2012).
- [104] A. Kuhn, A. Bourdon, J. Rigoult, and A. Rimsky, *Phys. Rev. B* **25**, 4081 (1982).
- [105] D. Errandonea, A. Segura, V. Muñoz, and A. Chevy, *Phys. Rev. B* **60**, 15866 (1999).
- [106] S. Benazeth, N.-H. Dung, M. Guittard, and P. Laruelle, *Acta Crystallogr. Sect. C* **44**, 234 (1988).
- [107] K. El-Sayed, Z. K. Heiba, K. Sedeek, and H. H. Hantour, *J. Alloys Compd.* **530**, 102 (2012).
- [108] D. Schiferl and C. Barrett, *Journal of Applied Crystallography* **2**, 30 (1969).
- [109] J. Q. Li, X. W. Feng, W. A. Sun, W. Q. Ao, F. S. Liu, and Y. Du, *Materials Chemistry and Physics* **112**, 57 (2008).
- [110] W. Chen, Z. Meng, J. Liang, L. Chen, and Y. Chen, *Sci. Sin.-Phys. Mech. Astron.* **50**, 047301 (2019).
- [111] K. D. Bronsema, J. L. D. Boer, and F. Jellinek, *Zeitschrift für anorganische und allgemeine Chemie* **540**, 15 (1986).
- [112] A. Laturia, M. L. Van de Put, and W. G. Vandenberghe, *npj 2D Mater Appl* **2**, 1 (2018).
- [113] A. Opalovskij and V. Fedorov, *Dokl. Akad. Nauk SSSR* **163**, 1163 (1965).
- [114] W. J. Schutte, J. L. De Boer, and F. Jellinek, *Journal of Solid State Chemistry* **70**, 207 (1987).
- [115] V. Kalikhman, *Inorg. Mater.* **19**, 957 (1983).
- [116] A. Yanaki and V. Obolonchik, *Inorg. Mater.* **9**, 1855 (1973).
- [117] W. S. Kim, G. Y. Chao, and L. J. Cabri, *Journal of the Less Common Metals* **162**, 61 (1990).
- [118] G. Kliche, *Journal of Solid State Chemistry* **56**, 26 (1985).
- [119] J. Du, P. Song, L. Fang, T. Wang, Z. Wei, J. Li, and C. Xia, *Applied Surface Science* **435**, 476 (2018).
- [120] D. T. Hodul and A. M. Stacy, *Journal of Solid State Chemistry* **54**, 438 (1984).
- [121] R. Yue, A. T. Barton, H. Zhu, A. Azcatl, L. F. Pena, J. Wang, X. Peng, N. Lu, L. Cheng, R. Addou, *et al.*, *ACS nano* **9**, 474 (2015).
- [122] H. Wiedemeier and H. Goldman, *Journal of the Less Common Metals* **116**, 389 (1986).
- [123] R. M. Hazen and L. W. Finger, *American Mineralogist* **63**, 289 (1978).
- [124] Y. Kumagai, L. A. Burton, A. Walsh, and F. Oba, *Phys. Rev. Applied* **6**, 014009 (2016).
- [125] G. Busch, C. Fröhlich, F. Hulliger, and E. Steigmeier, *Helv. Phys. Acta* **34**, 359 (1961).
- [126] H. Wang, Y. Gao, and G. Liu, *RSC Advances* **7**, 8098 (2017).
- [127] M. I. B. Utama, R. J. Koch, K. Lee, N. Leconte, H. Li, S. Zhao, L. Jiang, J. Zhu, K. Watanabe, T. Taniguchi, *et al.*, *Nature Physics* **17**, 184 (2021).
- [128] S. Lisi, X. Lu, T. Benschop, T. A. de Jong, P. Stepanov, J. R. Duran, F. Margot, I. Cucchi, E. Cappelli, A. Hunter, *et al.*, *Nature Physics* **17**, 189 (2021).
- [129] C. H. Stansbury, M. I. B. Utama, C. G. Fatuzzo, E. C. Regan, D. Wang, Z. Xiang, M. Ding, K. Watanabe, T. Taniguchi, M. Blei, *et al.*, *Science advances* **7**, eabf4387 (2021).